MRS Proceedings – 2012 IMRC Meeting. Symposium S6B. Low-Dimensional Semiconductor Structures. Volume 1534. p007 (6 pages) (2013). doi:10.1557/opl.2013.295.

Iron Silicide Nanostructures Prepared by E-Gun Evaporation and Annealing on Si(001)

György Molnár[1], László Dózsa[1], Zofia Vértesy[1] and Zsolt J. Horváth[1,2]
[1]Institute of Technical Physics and Materials Science, Research Centre for Natural Sciences, HAS, Budapest, H-1525 P.O. Box 49, Hungary,
[2]Óbuda University, Kandó Kálmán Faculty of Electrical Engineering, Institute of Microelectronics and Technology, H-1084 Budapest,Tavaszmező u. 15-17, Hungary

ABSTRACT

Iron silicide nanostructures were grown on Si(001) by strain-induced, self-assembly method. E-gun evaporated iron particles were deposited both onto room temperature and high temperature Si substrates, and were further annealed in situ. The initial Fe thickness was in the 0.1-6 nm range and the annealing temperatures varied between 500 and 850°C. The phases and structures formed were characterized by reflection high energy electron diffraction and by scanning electron microscopy. The electrical characteristics were investigated by I-V and C-V measurements, and by deep level transient spectroscopy. The size distributions of the formed iron silicide nanostructures were not homogeneous but, were oriented in perpendicular directions on Si(001). Higher temperature annealing resulted in increased particles size and faceting. Electrical characteristics showed critical defect concentration related to Fe.

INTRODUCTION

New generation thin film solar cells have to use environmentally friendly, non toxic and abundantly available chemical elements [1]. One of the potentially candidates is semiconducting β-$FeSi_2$, which has 23% theoretical efficiency in solar cells. Efforts have been made to produce iron silicide based photovoltaic devices, since both in its thin film and nanoparticle shapes have potential applications in photovoltaic technology [2-4]. Terasawa and coworkers suggested a composite β-$FeSi_2$/Si film for solar cells use, where iron silicide nanoparticles are embedded in silicon. In this case photocarriers are generated in the iron silicide particles, which has high photoabsorption coefficient, while carrier transport happens in silicon. This kind of material may result an excellent, new solar cell as a consequence of its high photoabsorption coefficient and high carrier mobility [5].

β-$FeSi_2$ is an indirect semiconductor, although in epitaxial configurations it shows a direct band gap on silicon substrate due to lattice distortions [6,7]. During solid phase thin film reactions the following phases of the Fe-Si equilibrium phase diagram have found on Si substrates [8-11]: The mostly Fe-rich iron silicide is Fe_3Si (DO_3 type), with cubic lattice. Two types of iron monosilicides might be present in thin film form. The first monosilicide phase is ε-FeSi with cubic structure and the second phase is cesium-chloride type cubic FeSi. The iron disilicides might appear with three different crystal structures. The high temperature, metastable, tetragonal α-$FeSi_2$ phase might be present in thin film form on Si substrates. The cubic γ-$FeSi_2$

phase is also metastable. At the end, the stable β-$FeSi_2$ has orthorhombic structure. All of the above phases, including metastable ones, might be epitaxially stabilized on the surface of Si substrates [12].

The most effective physical method of nanostructure preparation is the self-assembly, that have been observed besides compound and group IV semiconductors in a wide range of material and substrate combinations [13]. The strain induced self-assembled growth is a basic physical procedure of preparation of the nanoscale objects. During the growth of strained layers, the film often remains planar up to a critical thickness that depends on the lattice mismatch of the film and the substrate. Above that critical thickness, three dimensional dislocation free islands may form [14]. This phenomenon is the Stransky-Krastanov transition, which is an important way of self-assembled formation of quantum dots and wires. That type of growth may occur during the growth of epitaxial silicides.

The motivation of this study is to compare the formation of iron silicide nanostructures prepared by (i) iron evaporation onto Si substrate, which is kept at room temperature (RT) with subsequent annealing and by (ii) reactive deposition epitaxy method (RDE), where the iron particles are evaporated onto heated Si substrates. This research field may contribute to gain new knowledge in design of the morphology of iron silicides, and for practical side to make new steps towards more effective environmentally friendly solar cells.

EXPERIMENT

Pieces of (001) oriented Si (p-type, 12-20 Ωcm) wafers were used as substrates. Before loading the samples into the oil free evaporation chamber their surfaces were etched in diluted HF. Prior to evaporation Si wafers were annealed in situ for 5 min at 850°C. Iron ingots of 99.9% purity were evaporated using an electron gun, at an evaporation rate of 0.01-0.03 nm/s, at a pressure of $3*10^{-6}$ Pa. The film thickness was measured by vibrating quartz. The temperatures were monitored by small-heat-capacity Ni-NiCr thermocouples. The initial Fe thicknesses were in the 0.1-6.0 nm range and the annealing temperatures varied between 500 and 850°C.

Samples were annealed by two methods: (i) Fe evaporation onto room temperature (RT) substrates with subsequent annealing for 60 minutes, (ii) reactive deposition epitaxy method (RDE), where the substrates were heated during Fe evaporation. The RDE grown samples were post annealed after the end of the deposition in situ in the vacuum chamber. The total annealing time (deposition + post annealing time) for the RDE grown samples were 60 minutes too. So, the thermal budget was the same for the differently prepared samples at a given temperature.

The growth processes were tracked in situ by reflection high energy electron diffraction (RHEED) at 10 keV beam energy during the sample preparation. The morphologic features of the nanostructures were characterized by scanning electron microscopy (SEM). The electrical characteristics were investigated by current-voltage (I-V), and capacitance-voltage (C-V) measurements and the defects were measured by deep level transient spectroscopy (DLTS).

DISCUSSION

The whole sample preparation process was followed up by in situ RHEED measurements. The azimuthal orientation of the 10 keV e-beams was along Si <110> for all of

the samples. In Fig. 1(a-e) can be seen the RHEED images of the two iron silicide samples, which were taken during sample preparation, where the deposited mass equivalent Fe thickness was 0.1 nm, and the heat treatment was carried out at 850°C for 60 minutes for both of the samples. The only difference is the deposition mode: The first column of images belongs to an RT deposited and then annealed sample and the second column to an RDE deposited and then further annealed sample for comparison. In Fig. 1(a-b) can be seen the RHEED images of the cleaned and annealed Si(001) substrate showing 2x1 reconstruction for both of the samples. Fig. 1(c-d) shows state of the surface after 0.1 nm iron evaporation. In case of the RT deposited sample (Fig. 1(c)) the original Si surface reconstruction disappeared and the lines weakened, as consequence of very thin Fe covering. While, the RDE deposited sample (Fig. 1(d)) shows promptly appeared new lines belonging to iron silicide phase formed on the hot substrate instantaneously. RHEED images of Fig. 1(e-f) show the state of the surfaces after annealing, where both images show a new, ordered surface with epitaxial character. The misfit differences of Si(001) and of the three iron disilicide phases, written in the introduction section, are within two percent [11] that is why the RHEED cannot differentiate between them.

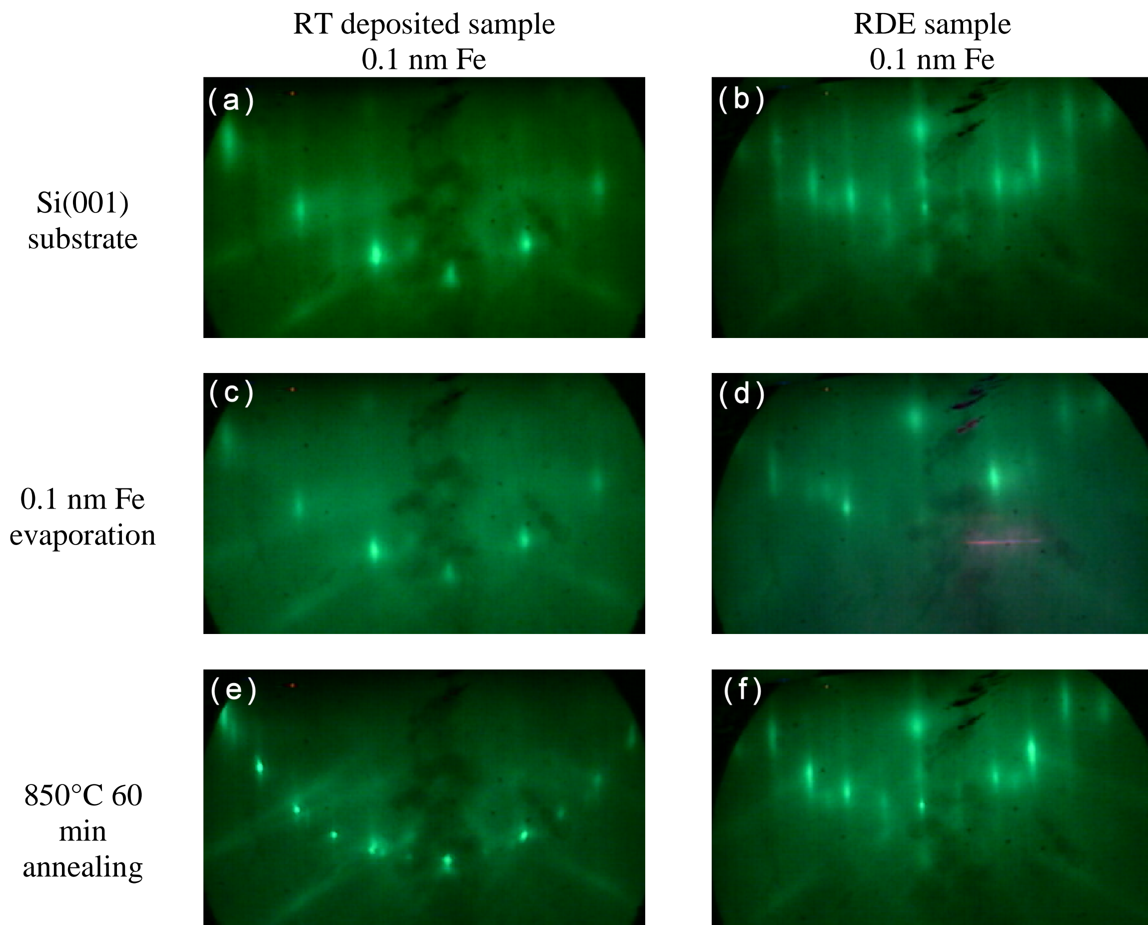

Figure 1. RHEED images iron silicide nanostructure formation. The first column belongs to an RT deposited sample and the second to an RDE ones. (a-b) Si substrate, (c-d) after 0.1 nm Fe deposition, (e-f) after 850°C 60 min annealing

MRS Proceedings – 2012 IMRC Meeting. Symposium S6B. Low-Dimensional Semiconductor Structures. Volume 1534. p007 (6 pages) (2013). doi:10.1557/opl.2013.295.

The particular phase identification of iron disilicide nanostructures by transmission electron microscopy selected area electron diffraction was presented for similar samples in a previous paper [15].

SEM images of iron silicide nanostructures are presented in Figs. 2(a-f) as a function of the annealing temperature. The first column of images shows the RT deposited and then annealed sample, the second column shows the RDE deposited and then further annealed sample for comparative study. The film thickness was 0.1 nm for each sample, and the heat treatments were carried out at 500, 600, and 850°C for 60 minutes. All of the samples show aggregated iron silicide nanostructures. The size and the distribution of the islands depend on the temperature and on the type of the annealing. At 500°C annealing; the density of the silicide nanostructures is higher for RT sample compared to RDE one (Fig. 2(a-b)). At 600°C annealing; besides the small nanostructures, bigger size aggregates appeared (Fig. 2(c-d)).

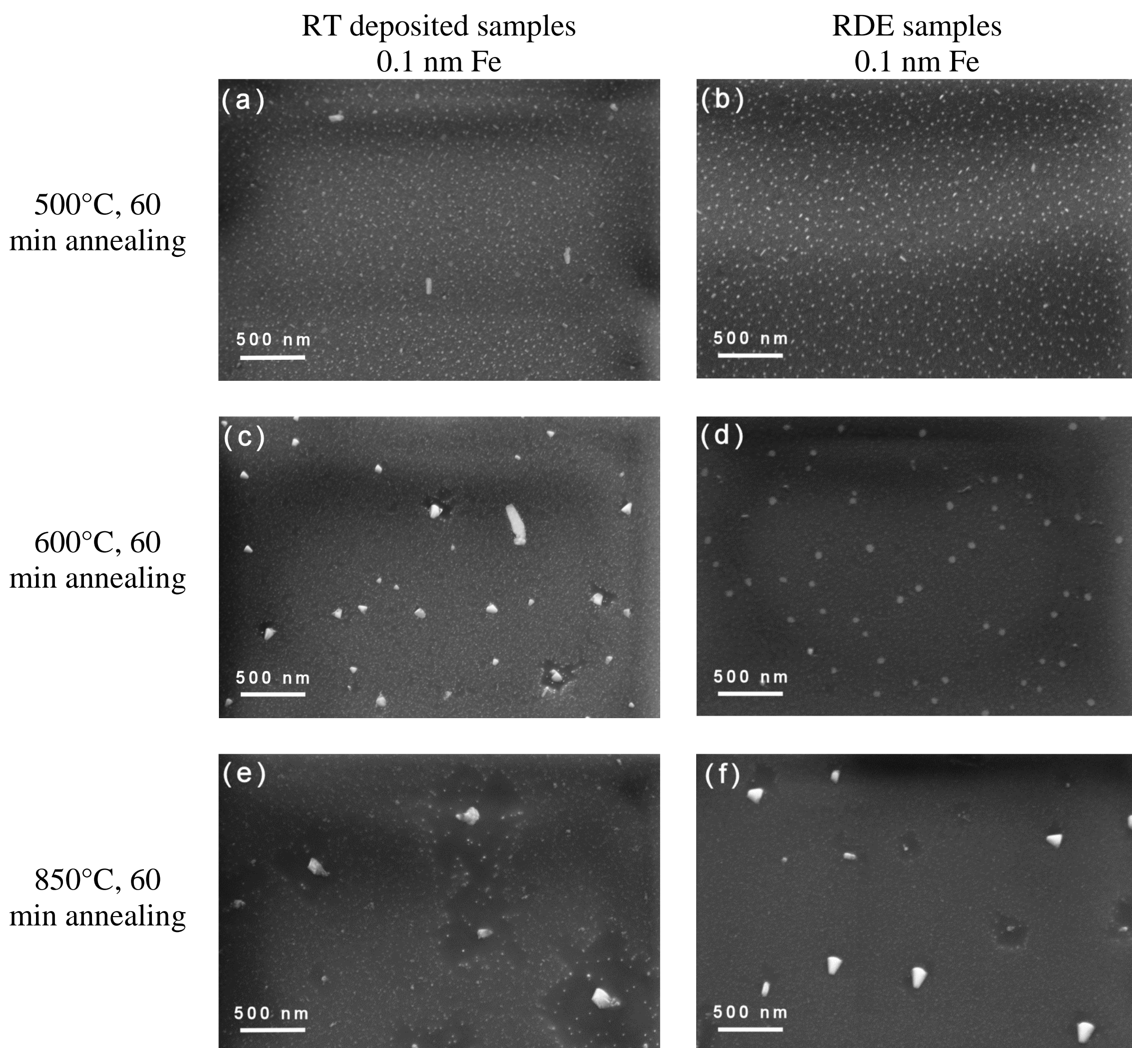

Figure 2. SEM images of iron silicide nanostructures formed at RT (first column) and RDE (second column) depositions at different temperatures for comparison. Samples annealed at (a-b) 500°C, (c-d) 600°C, (e-f) 850°C, for 60 minutes.

In case of RT sample the characteristic shape of big aggregates is the triangular, while for RDE sample the circle. At 850°C annealing the RT sample shows randomly shaped structures and the RDE sample shows perpendicularly ordered, triangular objects (Fig. 2(e-f)).The local environment of these big objects is depleted as a consequence of Ostwald ripening phenomena, where the bigger islands grow further at the cost of the smaller ones [16]. In case of thicker samples - up to 6 nm initial Fe thickness - the size of aggregated object grows continuously, reaching the 1 micrometer lateral dimensions.

According to electrical characteristics, the Fe related defects are dominant in all samples. Fig. 3(a-c). The current-voltage and capacitance-voltage characteristics show these defects in about 1-2 μm depth from the surface. The doping concentration determined from the C-V characteristics decreases near the surface. The deep level defects compensate the doping of the starting wafer. The I-V and C-V values has significant scatter in different junction, some of the junctions are dominated by leakage of the junctions in reverse bias. We assume it is due to the rough silicides/silicon interface morphology and to very large defect concentration in the vicinity of the interface.

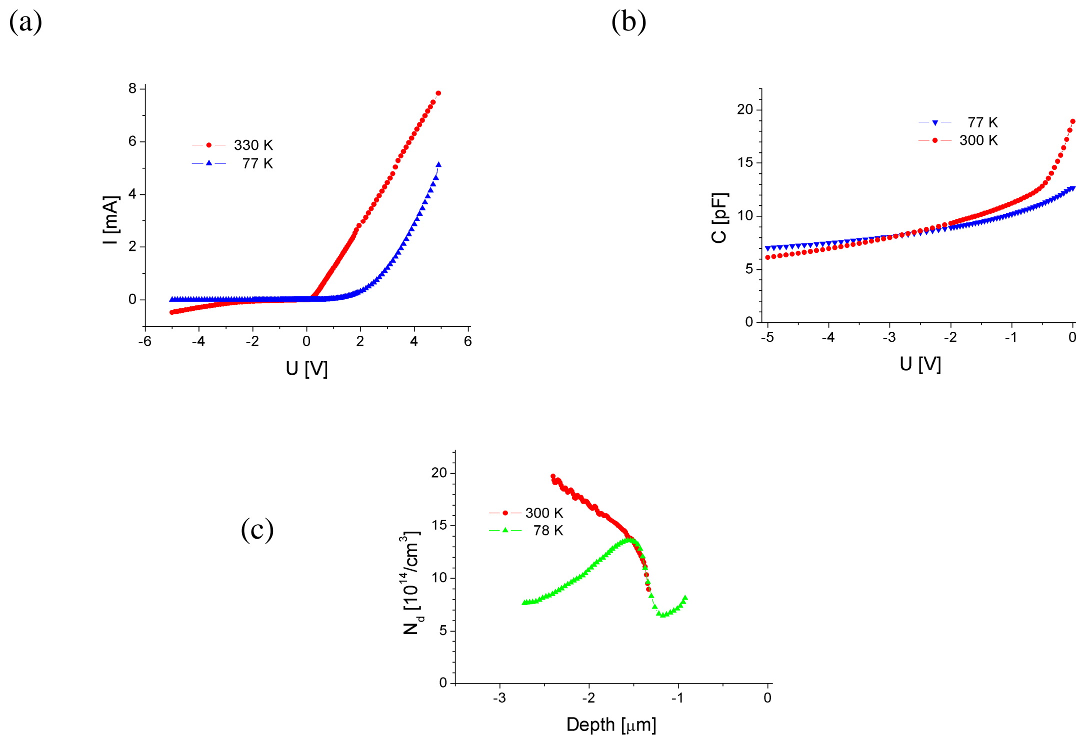

Figure 3. (a) Current-voltage plot, (b) capacitance–voltage plot, (c) depth profile of main defects of a 1 nm thick sample measured at temperatures indicated in the plots.

CONCLUSIONS

Iron silicide nanoislands were grown on Si(001) substrate by RT deposited and then annealed and by RDE deposited and then further annealed methods for comparison. The shape of

the nanostructures varied from circular to triangular and quadratic depending on the initial Fe thickness and on the annealing method and temperature. The size distribution of the formed iron silicide nanoobjects was not homogeneous, but they were oriented in perpendicular directions on Si(001). Higher temperature annealing resulted in increased particles size and faceting. The RT and RDE growth mode resulted similar nanostructures, no sharp difference was detected between them. Electrical characteristics show the critical problem for application, which is the large defect concentration related to Fe. In case of successful engineering of iron silicide nanostructures they might be used potentially as environmentally friendly semiconductors for more effective solar cells.

ACKNOWLEDGMENTS

The authors would like to thank the support of OTKA Grant No. 81998.

REFERENCES

1. F. Alharbi, J. D. Bass, A. Salhi, A. Alyamani, H. C. Kim, and R. D. Miller, Renew. Energ. **36**, 2753 (2011).
2. M. Shaban, K. Nakashima, W. Yokoyama, and T. Yoshitake, Jap. J. Appl. Phys. **46**, L667 (2007).
3. G. K. Dalapati, S. L. Liew, A. S. W. Wong, Y. Chai, S. Y. Chiam, and D. Z. Chi, Appl. Phys. Lett. **98**, 013507 (2011).
4. T. Buonassisi, A. A. Istratov, M. A. Marcus, B. Lai, Z. Cai, S. M. Heald, and E. R. Weber, Nature Materials **4**, 676 (2005).
5. S. Terasawa, T. Inoue, and M. Ihara, Solar Energy Materials & Solar Cells **93**, 215 (2009).
6. D. B. Migas, and L. Miglio, Phys. Rev. B **62**, 11063 (2000).
7. K. Yamaguchi, and K. Mizushima, Phys. Rev. Lett. **86**, 6006 (2001).
8. K. A. Mäder, H. von Känel, and A. Baldereschi, Phys. Rev. B **48**, 4364 (1993).
9. H. von Känel, K. A. Mäder, E. Müller, N. Onda, and H. Sirringhaus, Phys. Rev. B **45**, 13807 (1992).
10. N. Jedrecy, A. Waldhauer, M. Sauvage-Simkin, R. Pinchaux, and Y. Zheng, Phys. Rev. B **49**, 4725 (1994).
11. P. Villars, and L. D. Calvert, *Pearson's Handbook of Crystallographic Data for Intermetallic Phases*, Vol. 3, (American Society for Metals, Metals Park, OH 1985) p. 2232.
12. G. Molnár, L. Dózsa, G. Pető, Z. Vértesy, A. A. Koós, Z. E. Horváth, and E. Zsoldos, Thin Solid Films **459,** 48 (2004).
13. A. L. Barabási, Appl. Phys. Lett. **70**, 2565 (1997).
14. J. Tersoff, and F. K. LeGoues, Phys. Rev. Lett. **72,** 3570 (1994).
15. N. Vouroutzis, T. T. Zorba, C. A. Dimitriadis, K. M. Paraskevopoulos, L. Dózsa and G. Molnár, J. Alloys Compounds **448**, 202 (2008).
16. M. Zinke-Allmang, Thin Solid Films **346**, 1 (1999).
17. K. Wünstel, and P. Wagner, Appl. Phys. A **27**, 207 (1982).